Rapid Warming in Summer Wet Bulb Globe Temperature in China with Human-Induced Climate Change

Author(s): Chao Li, Ying Sun, Francis Zwiers, Dongqian Wang, Xuebin Zhang, Gang Chen and Hui Wu

Rapid Warming in Summer Wet Bulb Globe Temperature in China with Human-Induced Climate Change

Chao Li,[a,b] Ying Sun,[c,d] Francis Zwiers,[e,f] Dongqian Wang,[c] Xuebin Zhang,[g] Gang Chen,[h] and Hui Wu[b]

[a] Key Laboratory of Geographic Information Science (Ministry of Education), East China Normal University, Shanghai, China
[b] State Key Laboratory of Estuarine and Coastal Research, East China Normal University, Shanghai, China
[c] National Climate Center, Laboratory for Climate Studies, China Meteorological Administration, Beijing, China
[d] Collaborative Innovation Center on Forecast and Evaluation of Meteorological Disasters, Nanjing University of Information Science and Technology, Nanjing, China
[e] Pacific Climate Impacts Consortium, University of Victoria, Victoria, British Columbia, Canada
[f] Nanjing University of Information Science and Technology, Nanjing, China,
[g] Climate Research Division, Environment and Climate Change Canada, Toronto, Ontario, Canada
[h] Atmospheric and Oceanic Sciences, University of California, Los Angeles, California

ABSTRACT

On the basis of a newly developed observational dataset and a suite of climate model simulations, we evaluate changes in summer mean wet bulb globe temperature (WBGT) in China from 1961 through 2080. We show that summer mean WBGT has increased almost everywhere across China since 1961 as a result of human-induced climate change. Consequently, hot summers as measured by summer mean WBGT are becoming more frequent and more conducive to heat stress. Hot summers like the hottest on record during 1961–2015 in western or eastern China are now expected occur once every 3–4 years. These hot WBGT summers have become more than 140 times as likely in eastern China in the present decade (2010s) as in the 1961–90 baseline period and more than 1000 times as likely in western China. The substantially larger influence in western China is associated with its stronger warming signal, which is likely due to the high Bowen ratio of sensible to latent heat fluxes of dry soils and increases in absorbed solar radiation from the decline in mountain snow cover extent. Observation-constrained projections of future summer mean WBGT under the RCP8.5 emissions scenario indicate that, by the 2040s, almost every summer in China will be at least as hot as the hottest summer in the historical record, and by the 2060s it will be common (on average, every other year) for summers to be as much as 3.0°C hotter than the historical record, pointing to potentially large increases in the likelihood of human heat stress and to a massive adaption challenge.

1. Introduction

Significant increases in summer mean temperature since the mid-twentieth century in China have been observed and attributed to human influence (Ren et al. 2012; Sun et al. 2014; Wang et al. 2017). For example, it is reported that human influence has made the record-breaking hot summer of 2013 in eastern China more than 60 times as likely as it would have been in a natural world without human influence (Sun et al. 2014). Many cities documented excess deaths resulting from heat stress during this hot summer (Gao et al. 2015; Gu et al. 2016). In 2018, China experienced another record-breaking hot summer relative to historical annual national average summer mean temperatures since 1961 (CMA 2018).

While compelling, these studies and reports may not convey the full potential impacts of the changing frequency and intensity of heat events since they rely on dry air temperature measurements. Other climate factors, such as humidity and wind speed, may also influence

---

how humans feel heat stress (e.g., Sherwood and Huber 2010; Willett and Sherwood 2012; Fischer et al. 2012; Dunne et al. 2013; Zhao et al. 2015; Pal and Eltahir 2015; Knutson and Ploshay 2016; Li et al. 2017; Wehner et al. 2017; Coffel et al. 2018; Kang and Eltahir 2018). Heat stress occurs when the human body is not able to dissipate sufficient excess metabolic heat, leading to an increase in body core temperature. High humidity contributes to the likelihood of heat stress by reducing the ability to dissipate excess metabolic heat through the evaporation of sweat (e.g., Sherwood and Huber 2010; Goldie et al. 2015; Wehner et al. 2017). Unfortunately, the lack of good-quality long-term humidity observations has, until recently, limited the use of heat stress indicators that account for humidity, such as wet bulb temperature and wet bulb globe temperature (WBGT), in studies over large domains. While such indicators have been considered in several recent studies of heat-related hospitalization and mortality risk in specific jurisdictions (e.g., Ma et al. 2018; Heo and Bell 2018; Heo et al. 2019), those studies have not yet clarified whether the consideration of humidity helps to improve the identification of periods with heat-related health and mortality risk. Nevertheless, given the effect of humidity on the ability of the human body to dissipate heat, there is great value in studying WBGT from a climatological perspective over large domains.

A few detection and attribution analyses have now studied WBGT as an indicator of climatic conditions conducive to heat stress (e.g., Knutson and Ploshay 2016; Li et al. 2017), using the HadISDH observational records of near-surface temperature and humidity [Willett et al. 2014; HadISDH indicates a Met Office Hadley Centre–led project utilizing NOAA synoptic (hourly) Integrated Surface Database humidity data]. They report that summer climatic conditions, as indicated by increases in WBGT, have become more conducive to heat stress during the 1973–2012 period across the globe and that this long-term change would not have been observed if there had not been human influence on the climate. Based on a global-scale fingerprinting analysis, it has been further shown that the likelihood of occurrence of the observed record summer mean WBGT has increased by a factor of at least 70 over the 1973–2012 period in different regions of Northern Hemispheric land areas, with an extremely large increase in East Asia (which covers China; Li et al. 2017). Indeed, most regional record high WBGT summers occurred in the latter part of that period.

China is the most populous country in the world and has the world's second largest economy. Given the direct impacts of extreme heat events on the health of such a large population as well as other impacts such as on labor capacity and energy demand for air conditioning, it is important to focus a study of the historical

and projected future changes in summer WBGT specifically on China using improved observations and a regional-scale fingerprinting analysis. Previous studies for East Asia remain uncertain because data from the region are underrepresented in HadISDH. In addition, HadISDH only provides data from 1973 onward, whereas significant warming in China started since the mid-twentieth century (e.g., Sun et al. 2014; Wang et al. 2017). Also, summer temperatures in China have warmed substantially faster than the global mean summer land surface temperature (e.g., Sun et al. 2014). A global-scale fingerprinting analysis may therefore be too general to accommodate the more rapid warming in China.

Fortunately, a newly available dataset of quality-controlled and homogenized near-surface temperature and relative humidity observations from 2419 stations in mainland China for the period 1961–2015 (Cao et al. 2016) allows us to focus specifically on China. Using these data and the simulations from an ensemble of climate models participating in phase 5 of the Coupled Model Intercomparison Project (CMIP5; Taylor et al. 2012), we assess changes in China's summer mean WBGT from 1961 through 2080. This newly available temperature and humidity dataset, which has longer temporal coverage, starting both earlier and ending later than HadISDH, and more complete spatial coverage for China, represents summer WBGT changes over the country with substantially less observational uncertainty.

Here we first examine how observed summer mean WBGT has changed during the period of record. We then perform a fingerprinting analysis to determine whether the change can be attributed to human-induced climate change. The understanding of the causes of the observed summer WBGT change that is obtained in this way is used to constrain projections of future summer WBGT changes in China. In contrast to raw climate model projections that are not constrained by observations (e.g., Pal and Eltahir 2015; Coffel et al. 2018; Kang and Eltahir 2018), the observation-constrained projections are expected to be less prone to systematic climate model bias (e.g., Allen et al. 2000; Stott and Kettleborough 2002; Stott and Forest 2007; Gillett et al. 2012; Shiogama et al. 2016), thus providing more informative guidance for future heat stress adaptation planning in China.

Whereas a range of heat stress indicators have been developed to quantify human discomfort under hot and humid conditions (e.g., Buzan et al. 2015; Zhao et al. 2015; Zhu et al. 2019), we have recently adopted the use of WBGT (Li et al. 2017), motivated by a list of impact studies attributing reductions in industrial and military labor capacity and safety to heat stress increases in different regions around the world (e.g., Budd 2008; Hyatt et al. 2010; Dunne et al. 2013; Akihiko et al. 2014).

Moreover, WBGT is a heat index having known thresholds relating directly to levels of physical activity (Willett and Sherwood 2012). While daily WBGT can more closely reflect thermal conditions conducive to heat stress on humans, we study summer mean WBGT due to the lack of homogenized daily observations of relative humidity at the time of writing. Nevertheless, a first-order expectation is that a warming in seasonal mean WBGT would shift the distribution of daily WBGT to warmer levels, potentially leading to more heat days that are more conducive to heat stress if the daily variability of summer WBGT does not decrease significantly. Modeling evidence shows that changes in seasonal mean air temperature do drive changes in subseasonal heatwave frequency and intensity in most regions across the globe (Argüeso et al. 2016; Li et al. 2018). Understanding changes in summer mean WBGT and their causes is therefore relevant for informing future climatic conditions conducive to summer heat stress.

2. Data and preprocessing

We use quality-controlled and homogenized monthly observations of near-surface temperature and relative humidity from 2419 stations in mainland China for the period 1961–2015, provided by the National Meteorological Information Center of China (Cao et al. 2016). We compute monthly mean WBGT (°C) at each station as WBGT = 0.3TA + 0.7WBT, where TA is air temperature (°C) and WBT is wet bulb temperature (°C), similarly to a number of existing studies (e.g., Willett and Sherwood 2012; Fischer et al. 2012; Knutson and Ploshay 2016; Li et al. 2017). We use the estimator of Stull (2011) to calculate WBT from dry air temperature and relative humidity. Other more sophisticated estimators require additional variables such as wind speed, solar radiation, and surface pressure (e.g., Davies-Jones 2008; Liljegren et al. 2008; Lemke and Kjellstrom 2012; Buzan et al. 2015), while reliable observations and simulations for some of these variables are limited. Neglecting the effects of wind and solar radiation means that the resulting WBGT reflects well-shaded or indoor thermal conditions (without air conditioning). Also, we note that monthly WBGT values estimated from monthly temperature and relative humidity can be different from those estimated from daily data due to the nonlinear dependence of WBGT on temperature and humidity (Stull 2011). The influence was confirmed to be small with reanalysis data in Li et al. (2017).

For each station, we calculate summer (June–August) mean WBGT by averaging monthly values over the three summer months if at least two monthly values are available, and otherwise mark a summer as missing.

Summer WBGT anomalies relative to a 1961–90 baseline period are then computed for stations with at least 18 (60%) years of data during the baseline period, and are otherwise marked as missing. The resulting station anomalies are aggregated to $5° \times 5°$ grid cell anomalies by averaging all available station anomalies within a predefined grid cell. This gridcell system, which has also been used in previous studies investigating near-surface air temperature changes in China (e.g., Sun et al. 2014; Wang et al. 2017), allows relatively accurate estimates of spatial averages from uneven station observations. Grid cells with 44 (80%) or more years of data during 1961–2015 are retained for subsequent analysis.

We use CMIP5 historical simulations to estimate the response of summer mean WBGT to all known historical forcings combined (including both natural and anthropogenic components) and use CMIP5 naturalforcing simulations to estimate the response to the natural-forcing components (see Table S1 in the online supplemental material). We estimate the forced responses of summer WBGT to external forcing as the multimodel ensemble means of the corresponding simulations by averaging all available simulations for each model and then calculating the mean of the ensemble of model averages. To reduce the influence of internal variability on the estimated responses, we select climate models with ensembles of at least three simulations under a particular forcing that are directly available through to the year 2012, or that can be extended to 2012, which is the last year of the CMIP5 natural-forcing simulations. As many CMIP5 historical simulations end in 2005, we extend them to 2012 using simulations from either the CMIP5 historicalExt experiment, if available, or the corresponding simulations with forcings that follow the representative concentration pathway (RCP) 8.5 emissions scenario. To make full use of available observations to derive observational constraints for projecting future summer WBGT, we further extend these historical simulations to 2015 for one-signal fingerprinting analysis (see next section), which serves as a reference for constraining summer WBGT projections. The particular choice of RCP scenario for data extension is not important because different RCPs have similar radiative forcing during 2006–15 (IPCC 2013).

To estimate the internal variability in summer mean WBGT, we obtain a set of 285 55-yr segments of CMIP5 preindustrial control simulations from 33 climate models (supplemental Table S1). These 55-yr segments, which are the same length as the observed record (1961–2015), are assigned calendar dates by designating the first year in each segment as 1961. Grid cells are then made missing year-by-year as in the observations. To evaluate how summer mean WBGT will change in future, we use
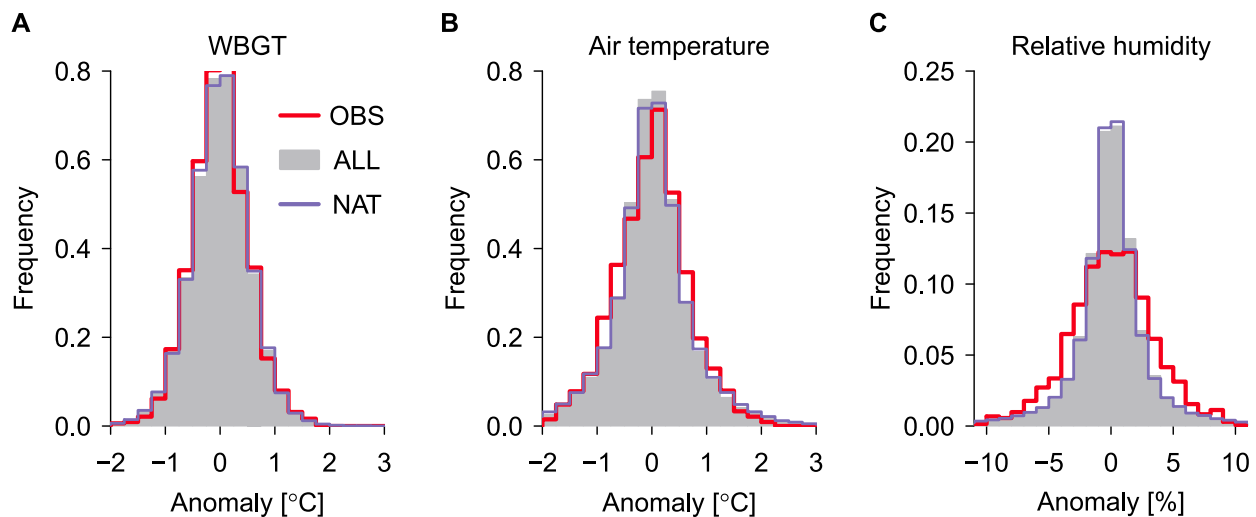
FIG. 1. Climate models reproduce the nonsecular variability of summer mean WBGT in mainland China, and the nonsecular variability in WBGT is smaller than in air temperature: histograms of the detrended 1961–2015 summer mean (a) WBGT, (b) dry air temperature, and (c) relative humidity for grid cells in mainland China produced from observations (red curves), CMIP5 historical simulations (gray bars), and historical natural simulations (blue curves).

CMIP5 projections up to 2080 under the RCP4.5 and RCP8.5 emissions scenarios from models that also provide simulations for estimating the forced response to all known historical forcings.

For all model simulations, we estimate summer WBGT with monthly air temperature and relative humidity on the models' native grid, convert the estimates to anomalies relative to 1961–90, and then regrid the anomalies to the $5° \times 5°$ grid of the observations using bilinear interpolation. We mask the resulting anomalies of historical and natural simulations as well as segments of control simulations by the availability of observations to ensure fair comparisons between observations and model simulations. We find that climate models successfully reproduce the observed nonsecular interannual variability in summer mean WBGT in China, that is, the variability in the detrended summer mean WBGT (Figs. 1a,d), even though models appear to undersimulate the nonsecular variability of summer mean relative humidity (Figs. 1c,f). This is not unexpected considering that WBGT variability is dominated by air temperature variability, for which there is also very good agreement between models and observations (Figs. 1b,e). Similarity of the secular component of the summer WBGT variability will be demonstrated in the subsequent detection and attribution analysis (section 4).

3. Methods

We use a space–time optimal fingerprinting method (Allen and Stott 2003; Ribes et al. 2013) to ascertain the role of anthropogenic influence in driving the observed long-term changes in summer mean WBGT and in developing record hot summers. This method projects the concatenated nonoverlapping 5-yr mean summer WBGT anomalies $\mathbf{y}$ during a historical period (e.g., 1961–2015) for western and eastern China (separated at 105°E as shown by the white line in Fig. 2b) onto corresponding estimates of summer WBGT responses to external forcings $\mathbf{x}$ as follows: $\mathbf{y} = \mathbf{x}\boldsymbol{\beta} + \boldsymbol{\varepsilon}_\mathbf{y}$, where $\mathbf{x} = \mathbf{x}^* + \boldsymbol{\varepsilon}_\mathbf{x}$. The residual vector $\boldsymbol{\varepsilon}_\mathbf{y}$ and matrix $\boldsymbol{\varepsilon}_\mathbf{x}$ represent, respectively, internal variability in the observations and in the estimates of the forced responses in summer mean WBGT. Here $\mathbf{x}^*$ represents the unknown, but deterministic, forced responses in summer mean WBGT from climate models, whereas $\mathbf{x}$ is the multimodel mean estimate of $\mathbf{x}^*$, which is affected by climate-model-simulated internal variability. The scaling factors $\boldsymbol{\beta}$ and signals $\mathbf{x}^*$ are estimated using a total least squares approach (Ribes et al. 2013). Responses to external forcings are deemed to have been detected in the observations if the scaling factors are greater than zero at the 5% significance level. In these cases, scaling factors that are consistent with unity provide evidence that the estimated responses by climate models agree with the observations and therefore help to support attribution of the causes of observed changes.

We choose to perform a space–time analysis to accommodate the different warming rates in western and eastern China, as will become apparent later. We do not consider separate analysis for each region to reduce the potential for overfitting. We perform a two-signal analysis of the period 1961–2010 that involves signals describing the response to all known historical forcings
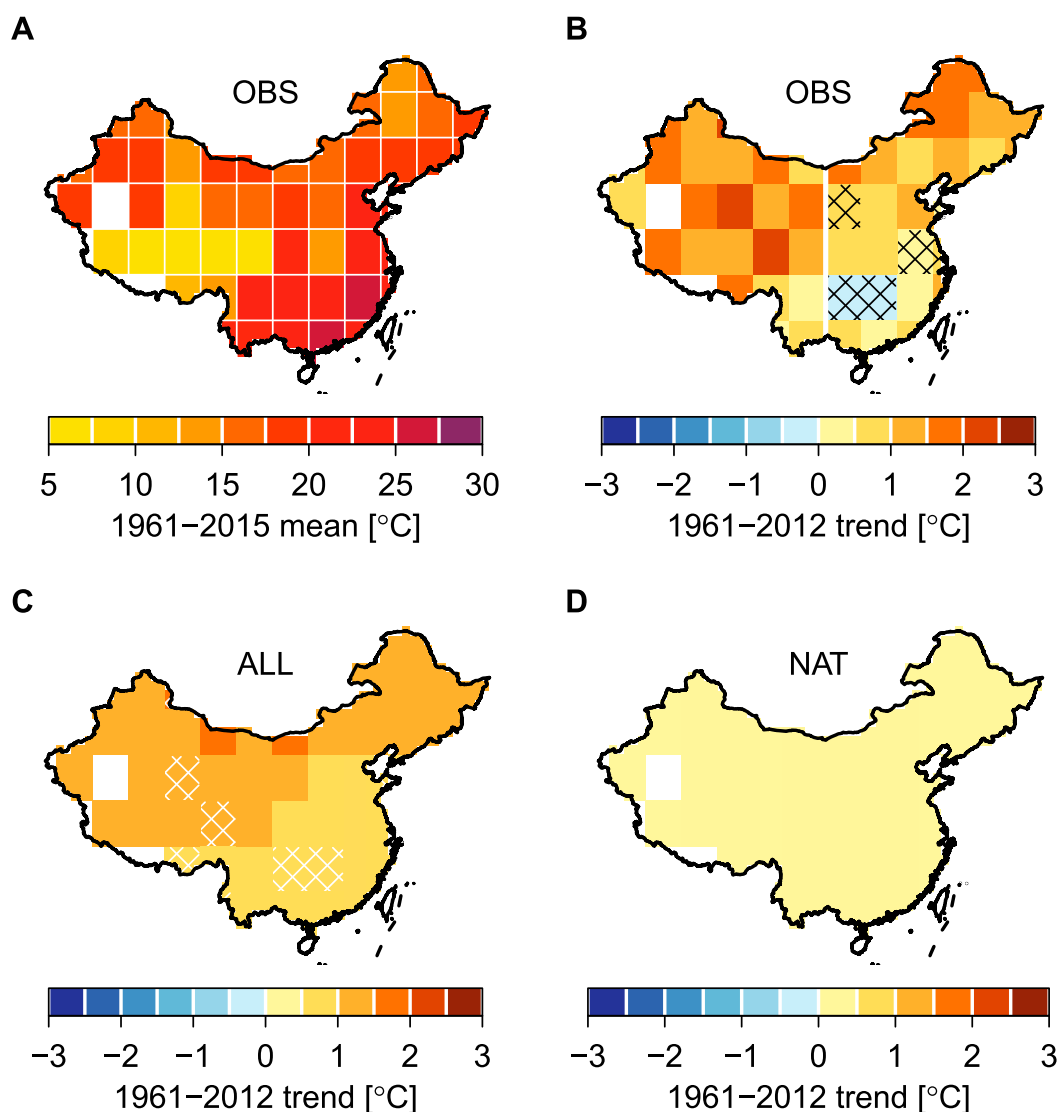
FIG. 2. Climatology and trend in summer mean WBGT in mainland China: (a) the observed 1961–2015 average of summer mean WBGT and the 1961–2012 summer mean WBGT trends in (b) observations and in the multimodel ensemble means of CMIP5 (c) historical and (d) natural-forcing simulations. Because the natural-forcing simulations end in 2012, trends are computed for the 1961–2012 period to ensure a fair comparision. Hatching in (b) marks grid cells for which the observed trends are *not* statistically significant at the 5% level as based on the Mann–Kendall test considering the influence of serial correlation, and the white line in (b) shows the boundary for defining western and eastern China. Hatching in (c) marks grid cells where the observed trends lie outside the ranges of trends in the ensemble means of the historical simulations of individual models. White grid cells have insufficient observations.

combined and the response to natural forcing only. We also perform a one-signal analysis of the period 1961–2015 where the signal of interest is the combined response to all known historical forcings.

The two-signal analysis aims to determine if anthropogenic influence can be detected in the observed summer mean WBGT changes (which is the case, as will become obvious later), and to further separate the anthropogenic and natural contributions to the observed changes. In the two-signal analysis, we derive estimates of scaling factors for the anthropogenic-forcing and natural-forcing signals based on an assumption that the summer mean WBGT response to all known historical forcings (ALL) can be linearly decomposed into responses to anthropogenic forcing (ANT) and to natural forcing (NAT; see details in Li et al. 2017). We exclude 2011 and 2012 to ensure that each 5-yr mean anomaly represents a complete 5-yr period. A two-signal analysis

that includes 5-yr mean anomalies for 2011–15 is not possible because the CMIP5 historical natural-forcing simulations end in 2012.

The one-signal analysis is used to obtain guidance for adjusting native model simulations of historical and future summer mean WBGT when producing observation-constrained historical reconstructions and future projections. These adjustments are made by assuming that the fractional difference between simulations and observations stays constant with time under future external forcings that are increasingly dominated by greenhouse gas forcing. To make full use of available observations, we consider the full 1961–2015 period using extended historical simulations. Using the one-signal analysis as a basis for constraining model simulations has a number of advantages. First, it involves the ALL signal only, and thereby avoids uncertainty in the NAT scaling-factor estimate, which is large. Second, the one-signal analysis allows us to use a longer observational period to estimate the ALL scaling factor, which reduces scaling-factor uncertainty relative to that estimated from a shorter record. Natural-forcing simulations of the future are not available in the CMIP5 archive, making the application of the two-signal regression model to future periods infeasible.

The estimated scaling factors can be used in two ways, that is, to quantify the contributions of anthropogenic or natural forcing to the observed summer WBGT trends, and to construct distributions of trends that might plausibly have been observed in the historical period given the estimated response to forcing and the influence of internal variability. The latter allows us to compare the likelihood of the observed trend in a naturally forced world and in a world forced by anthropogenic influence by comparing the corresponding distributions of plausible trends. The distributions of plausible trends are estimated from a large sample of observation-constrained reconstructions of nonoverlapping 5-yr mean anomaly time series for the period 1961–2010 in a naturally or anthropogenically forced world based on the two-signal analysis.

To make observation-constrained reconstructions, we first repeatedly add one of the 285 segments of 5-yr mean anomaly time series of preindustrial control simulations scaled by $1/(\text{ne}_S)^{1/2}$ to the estimated summer WBGT response to natural or anthropogenic forcing, where ne_S is the equivalent ensemble size (or degrees of freedom) that is appropriate to the estimated response to a given forcing S = ALL, ANT, or NAT. This step produces 285 plausible summer mean WBGT responses to each forcing scenario in the presence of internal variability. For the response to natural forcing, which is estimated directly from climate model simulations as the

multimodel ensemble mean with each model having equal weight, the equivalent ensemble size is calculated as $\text{ne}_{\text{NAT}} = N^2/\sum_{i=1}^{N}(1/N_i)$, where N is the number of climate models and N_i is the number of ensemble simulations from model i (e.g., Huntingford et al. 2006; Jones et al. 2013; Li et al. 2017). For the response to anthropogenic forcing, which is estimated as the difference between responses to all known forcings and natural forcing that are obtained from ensembles with different equivalent ensemble sizes ne_{ALL} and ne_{NAT}, the equivalent ensemble size is calculated as $\text{ne}_{\text{ANT}} = \text{ne}_{\text{ALL}}\text{ne}_{\text{NAT}}/(\text{ne}_{\text{ALL}} + \text{ne}_{\text{NAT}})$ (e.g., Christidis et al. 2012; Li et al. 2017). We scale these 285 plausible responses by each of 1000 plausible estimates of corresponding scaling factors generated from the two-signal analysis to account for uncertainty in the estimated scaling factors. This results in 285×1000 realizations of observation-constrained responses to either natural or anthropogenic forcing. These observation-constrained responses are then added repeatedly to each of the 285 segments of control simulations, producing a sample of $285 \times 1000 \times 285$ observation-constrained reconstructions of 5-yr mean anomaly time series for 1961–2010 for plausible trends estimation. The Sen's slope estimator is used for trend estimation (Sen 1968).

We evaluate the extent to which anthropogenic influence since 1961 has altered the occurrence of hot summers measured by summer mean WBGT using the probability ratio (PR), defined as P_2/P_1, and the fraction of attributable risk (FAR), defined as $(P_2 - P_1)/P_2$, where P_1 and P_2 are the estimated probabilities of summer WBGT exceeding a high threshold, such as the record value observed during 1961–2015, in the 1961–90 baseline period, and in a recent decade such as 2006–15, respectively. We estimate these probabilities with observation-constrained probability distributions of summer mean WBGT during the corresponding periods. To that end, we use a set of $285 \times 1000 \times 285$ observation-constrained 5-yr mean anomaly time series reconstructed following exactly the same procedure described above, but using extended historical all-forcing simulations (to 2015) and scaling factors from the one-signal analysis. We assume that the probability distribution of interannual variability of summer mean WBGT within a given 5-yr period can be represented by a Gaussian distribution with a center that depends on an observation-constrained value of the 5-yr mean anomaly and a standard deviation representing the year-to-year variability of summer WBGT. This standard deviation, which is estimated from control simulations, is about 0.29°C for both western and eastern China and is close to that of the 1961–2015 summer WBGT observations after removing a linear trend in both regions (0.29 for western China and 0.30 for eastern

China). Last, the distribution of annual summer mean anomalies for a given period (e.g., 1961–90 or 2006–15) is obtained as a mixture of $M = 1000$ 5-yr specific Gaussians where the 1000 centers are drawn at random from the sample of reconstructed 5-yr mean anomalies in the given period. The latter consists of $285 \times 1000 \times 285 \times m$ 5-yr mean anomalies, where m is the number of nonoverlapping 5-yr segments during that period (e.g., $m = 6$ for 1961–90 and $m = 2$ for 2006–15). Repeating the sampling procedure 500 times yields 500 plausible estimates for the probability distribution of annual summer mean WBGT values in the given period, which are used to estimate exceedance probabilities, PRs, FARs, and their uncertainties. The relatively complex sampling procedure described above was designed to ensure that the effects of multiple sources of uncertainty such as scaling-factor uncertainty and uncertainty due to internal variability in observations and model responses are reflected in our assessment of the probabilities, PRs and FARs.

To obtain insights into how summer mean WBGT is projected to change in future, we consider changes over time in the probability of exceeding the record summer mean WBGT value observed during the 1961–2015 period of record, by comparing event probabilities in the 1961–90 base period with event probabilities in the coming decades based on observation-constrained summer WBGT probability distributions for each future decade until the 2070s (2071–80) under the RCP4.5 and RCP8.5 emissions scenarios. Changes are described using both the probability ratio and return period length, where the return period length is simply the inverse of probability. Since both the risk ratio and return period saturate to constant levels as global warming progresses, they become uninformative beyond the warming level at which saturation occurs. We therefore also present the change of the observation-constrained probability distributions in each future decade.

4. Results and discussion

a. China's summer WBGT in the historical period

Figure 2a presents the 1961–2015 observed climatological summer mean WBGT. As expected, southeastern China has higher climatological summer WBGT than elsewhere because of its high temperature and high relative humidity, whereas the Tibetan Plateau has the lowest values benefiting from its high elevation (Fig. 2a). In contrast to WBGT, high climatological summer air temperatures are also found in the semiarid and arid regions of northwestern China (Fig. S1A in the online supplemental material), where the air is relatively dry (Fig. S1D). This contrast points to the importance of

relative humidity in exacerbating thermal conditions conducive to heat stress by high temperatures.

Almost all of China has experienced significant warming in summer WBGT over the 1961–2012 period, with greater warming in northern than in southern China and greater warming in western China than in eastern China (Fig. 2b). This spatial trend pattern is also present in summer air temperature (Fig. S1B), indicative of the dominant role of the rising air temperature in producing the widespread summer WBGT warming. Aggregated by area-weighted averaging over all grid cells with sufficient data, the upward evolution of the national average summer WBGT closely matches that of summer air temperature. In contrast, relative humidity exhibits little trend overall (Fig. S2 in the online supplemental materials) with a poorly defined spatial pattern of increases and decreases (Fig. S1E).

The north–south gradient of the summer WBGT trends is consistent with the expected pattern of response to greenhouse gas forcing, with more rapid warming over land at higher latitudes than at lower latitudes (Cai and Lu 2007; Wan et al. 2015). The larger increases in summer WBGT in northwestern China can be related to the high Bowen ratio (of sensible to latent heat fluxes) of the dry soils in those semiarid and arid inland regions, which leads to warmer surface air temperatures due to restricted evaporation from dry soils. The physical reasons for the enhanced WBGT warming in the Tibetan Plateau may include increases in absorbed solar radiation caused by decreases in snow cover extent (e.g., Ghatak et al. 2014; Pepin et al. 2015).

The multimodel ensemble mean summer mean WBGT changes during 1961–2012 under the combined natural and anthropogenic forcings also exhibit warming trends across China, with the spatial pattern of the trends being similar to that observed (Fig. 2c). The observed trends lie within the range of trends in the ensemble means of simulations of individual models in all grid cells except some isolated outliers where the observations show weak cooling trends and a few grid cells in the Tibetan Plateau (hatching in Fig. 2c). By contrast, the observed trends remain above the range of the trends under natural-only forcing over the majority of the grid cells (not shown), which show a weak and statistically insignificant warming trend in the multimodel ensemble mean (Fig. 2d).

Regions with statistically significant warming trends are somewhat more widespread in WBGT than in air temperature (Fig. 2b vs supplemental Fig. S1B). This is because the former has a larger warming-to-noise ratio than the latter due to its smaller internal variability (not shown). The smaller internal variability in WBGT is a result of the modulation effects of relative humidity on air temperature that results from the

negative interaction between the two variables (whose correlation coefficient is −0.48 on average over China).

There is also generally better consistency between the observed and simulated historical trends for summer WBGT than for air temperature (Fig. 2c vs Fig. S1C). This is also, in part, due to the negative correlation between air temperature and relative humidity. It has previously been noted that CMIP5 models that warmed more also tended to simulate stronger reductions in relative humidity, and vice versa (e.g., Fischer and Knutti 2012). Given their negative correlation, the effect of model biases in the two variables would tend to cancel each other in WBGT. It is therefore not surprising to see the better performance of models in reproducing the nonsecular variability (Fig. 1a) and secular trends (Fig. 2b) for summer mean WBGT than for the individual variables (Fig. 1b and Figs. S1C and S1F).

b. Causes of the changes in China's summer WBGT

We now present results from fingerprinting analyses confirming statistical evidence for the role of human influence in the observed long-term WBGT increase. We perform a space–time fingerprinting analysis, with two space dimensions representing respectively western and eastern China (separated at 105 °E as shown by the white line in Fig. 2b), by concatenating the nonoverlapping 5-yr mean summer WBGT anomalies for western and eastern China together. This ensures that an important aspect of the spatial pattern of observed change (Fig. 2b) is retained while keeping the dimensionality of the fingerprinting analysis manageable. Also, this particular spatial dimension reduction is of practical importance, since it contrasts a region that is intensely urban and very densely populated (eastern China) and another (western China) that tends to be opposite in these regards.

In both regions, the 5-yr running mean time series of regional average observed summer mean WBGT anomalies relative to 1961–90 (red lines in Fig. 3) show overall warming trends modulated by natural climate fluctuations (e.g., ENSO) and marked cooling responses to the 1982 El Chichón and 1991 Mount Pinatubo volcanic eruptions. These observed regional trends agree with the multimodel ensemble mean changes under anthropogenic and natural forcings combined (red lines vs white lines and gray envelopes in Fig. 3) but do not agree when the anthropogenic forcings are absent (red vs blue lines in Fig. 3), consistent with the comparisons at gridcell scales (Fig. 2).

The two-signal analysis reveals that anthropogenic influence is detectable in the observations at the 5% significance level (orange boxplot in Fig. 4a), while natural influence is not detectable at this significance level (blue boxplot in Fig. 4a), providing evidence for
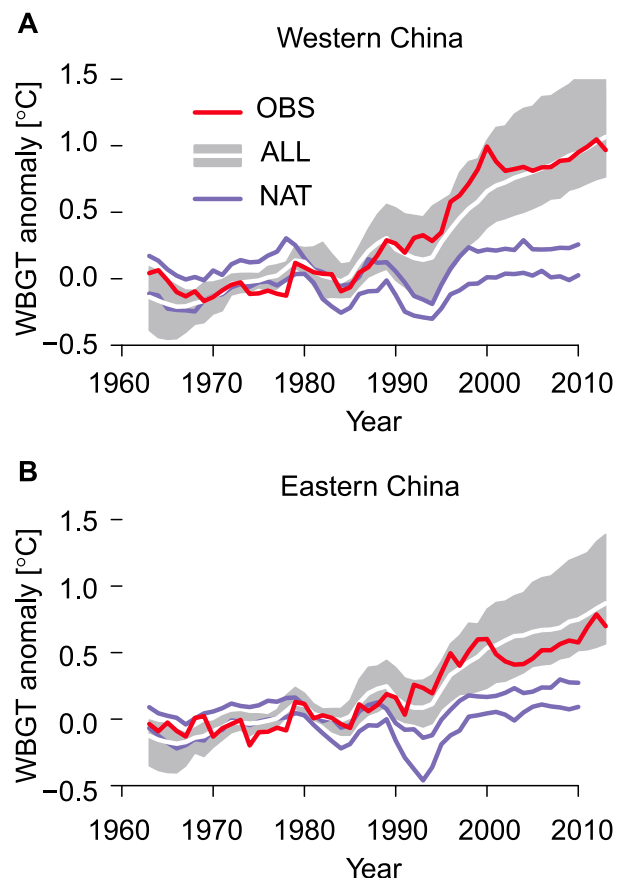

FIG. 3. Observed and simulated 5-yr running mean summer mean WBGT: time series of regional average 5-yr running mean summer mean WBGT anomalies in (a) western and (b) eastern China for observations (OBS; red line) and for CMIP5 historical simulations (ALL; white line for multimodel ensemble mean and gray shading for range of ensemble means of individual models) and natural-forcing simulations (NAT; blue lines for the range of ensemble means of individual models).

the dominant anthropogenic role in the observed summer WBGT warming in China. The best estimate of the ANT scaling factor is slightly greater than 1, suggesting that models somewhat underestimate the response to anthropogenic forcings. The use of a 5- or 10-yr time window for filtering internal variability does not strongly affect the regression results (not shown).

We estimate that summer mean WBGT increased by 1.17°C during 1961–2010 in western China and by 0.70°C in eastern China. Based on the two-signal analysis, we find that these trends would be exceptionally unlikely (<1% chance) to occur if there were no anthropogenic influence on the climate, particularly in western China, as indicated by the observation-constrained plausible summer WBGT trends in a naturally forced world, which are more or less 0 and well separated from the observed trends (dashed vertical lines vs blue histograms
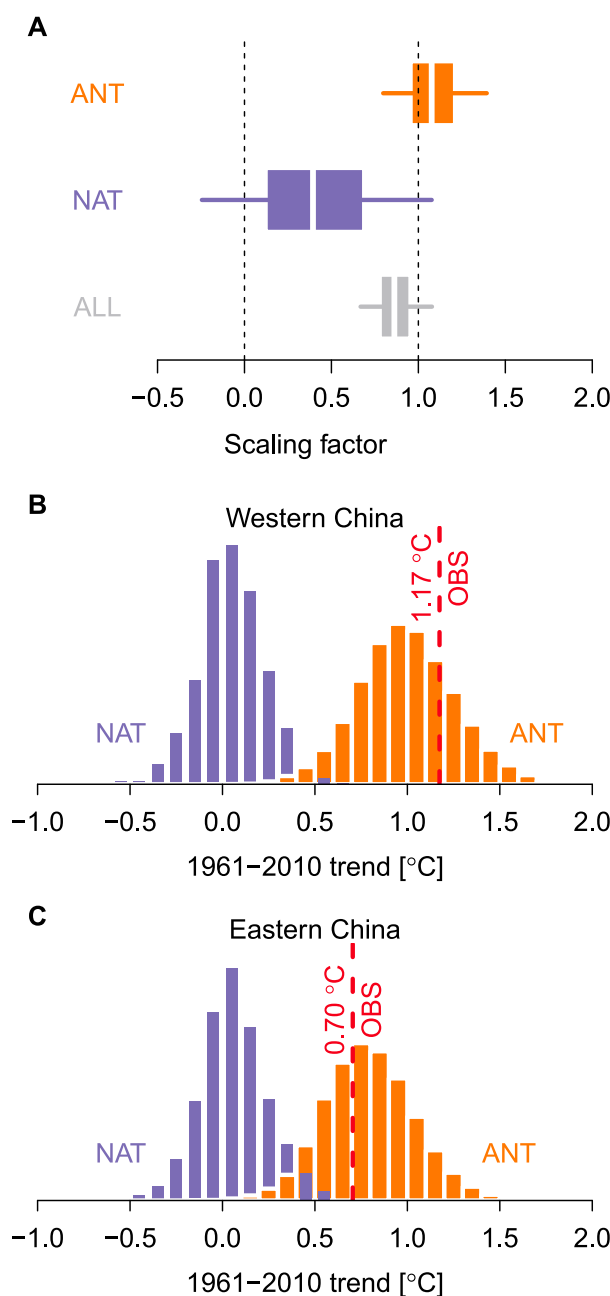
FIG. 4. Climatic conditions that are increasingly conducive to summer heat stress as measured by summer mean WBGT in China have human-induced origins: (a) Estimates of scaling factors for one-signal (ALL; gray) and two-signal (ANT and NAT; colors) fingerprint analyses. The white lines mark the scaling-factor best estimates. The width of the boxplot represents the 25%–75% uncertainty ranges of the scaling-factor estimates, and the whiskers extend to the 5%–95% uncertainties ranges. Also shown are trend histograms of the observation-constrained 1961–2010 summer mean WBGT in a climate with anthropogenic-only forcings (orange) and with natural-only forcings (blue) for (b) western and (c) eastern China. The observed trends are marked by vertical red lines.

in Figs. 4b and 4c). This contrasts with the plausible trends in a world affected by anthropogenic forcing only, which reproduce the observed trends in the central parts of the distributions of plausible trends (dashed vertical lines vs orange histograms in Figs. 4b and 4c). Overall, our results show that climate conditions that are becoming more conducive to high WBGT temperatures in China, which would tend to exacerbate potential heat stress risk, due mainly to anthropogenic influence.

As the contribution of natural forcing to the observed summer WBGT changes is confirmed to small in the two-signal analysis, we conduct a one-signal analysis involving the ALL signal only, and use it as a basis for evaluating the extent to which the long-term historical warming has altered the likelihood of extreme summer mean WBGT and to constrain projections of future summer WBGT. The 5%–95% confidence interval of the estimated ALL scaling factor lies well above 0 and is nearly centered on 1 (gray boxplot in Fig. 4a), which means that the modeled response to all known historical forcings is consistent with the observations at the 10% significance level, confirming again the limited role of natural forcing in the observed summer WBGT changes in China.

It is possible, however, that the good agreement between observations and models is partially, and serendipitously, affected by compensating biases in the observations and in the model-simulated response to all known historical forcings. Studies have reported that climate models tended to simulate greater-than-observed warming in global mean temperature during the last decade (e.g., Fyfe et al. 2013a), in part because model simulations from 2005 onward employ assumed external forcings that favor warming (e.g., Fyfe et al. 2013a; Medhaug et al. 2017), for example, by not including sufficient stratospheric aerosol forcing associated with volcanic activity after 2005 (e.g., Fyfe et al. 2013b; Ridley et al. 2014). On the other hand, China's rapid urbanization has contributed to the warming recorded in China's temperature data because of the preponderance of observing locations that are affected by expanding urban heat islands (e.g., Ren and Zhou 2014; Sun et al. 2016, 2019; Liao et al. 2018). This implies that the "apparent warming" in the observed summer WBGT may somewhat overestimate WBGT change for China's land area as a whole. It is, therefore, not impossible that the close agreement between observations and models is in part due to such compensating biases. Unfortunately, it is not possible to compare the magnitudes of these two biases in the present study.

c. Anthropogenic influence on China's record-high summer WBGT

We find that anthropogenic influence has strongly affected the occurrence of extreme summer mean heat

A

Western China

— 1961–1990
— 2006–2015
— 2011–2020

WBGT anomaly [°C]
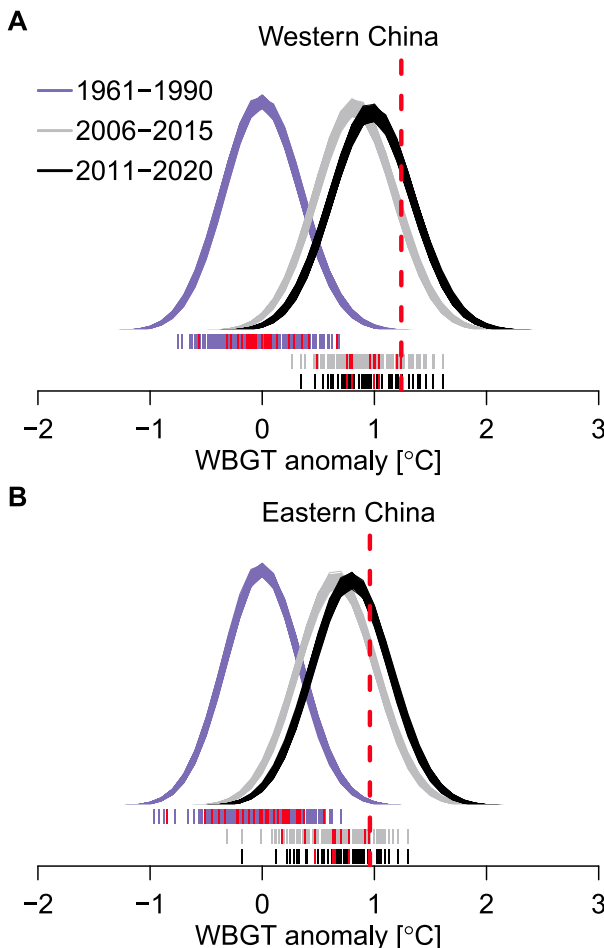
B

Eastern China

WBGT anomaly [°C]

FIG. 5. Human influence has strongly affected the occurrence of record hot summers measured by summer mean WBGT: observation-constrained probability distributions of summer mean WBGT during the 1961–90 baseline period (blue curves) and the recent 2006–15 (gray curves) and 2011–20 decades (black curves) for (a) western and (b) eastern China. For each period, there are 500 probability density curves, with one for each observation-constrained probability distribution. Red ticks show the observed summer mean WBGT during the three periods, and other ticks show reconstructed summer mean WBGT as based purely on observations for the three periods, as described in the text. Vertical red lines show the record summer mean WBGT experienced during 1961–2015.

conditions by shifting the probability distribution of summer mean WBGT in recent decades to hotter regimes relative to the 1961–90 baseline period (e.g., for 2006–15 and 2010–20, shifting in Fig. 5 from the blue curve to the gray and black curves respectively). The hottest summer on record as measured by summer mean WBGT during 1961–2015 occurred in 2012 with an anomaly of 1.24°C relative to the 1961–90 climatology in western China, and in 2013 with an anomaly of 0.96°C in eastern China (dashed vertical lines in Fig. 5). Based on observation-constrained probability distributions of

summer WBGT, the record hot summer events in western and eastern China were one-in-4377-year (3053–6450 years) and one-in-416-year (336–510 years) events during the 1961–90 baseline period, as opposed to an event occurring once every 3–4 years in the present 2011–20 decade for both regions.

The fact that the return period for the record hot summer event is similar in each region during the present decade facilitates the comparison of the PRs and FARs between the two regions, with a larger PR therefore indicating relatively greater rarity of the event during the baseline period. This is consistent with the suggestion of Harrington and Otto (2018) that regional events should be chosen so that the counterfactual probabilities are equal, except that in this case the factual probabilities are similar. Consideration of whether events should be defined so that factual or counterfactual probabilities are similar is analogous to selecting a base period for temperature anomaly evaluation. We, fortuitously, have a situation where the record events in both regions have similar probabilities in the current climate. This aids stakeholder communication since these are events that stakeholders have experienced directly.

Apparently, human influence since 1961 has made the observed record high WBGT summers about 1100 and 140 times as likely relative to the baseline period in western and eastern China, respectively, assuming limited natural influence, as we have already confirmed. The best estimates of the corresponding FARs are about 0.99 for both regions. These PR and FAR estimates are broadly consistent with those reported for summer mean WBGT in East Asia and the Tibetan Plateau based on the HadISDH dataset (Li et al. 2017). But they are an order-of-magnitude larger than those for summer air temperature such as that reported in Sun et al. (2014) for the 2013 record-breaking hot summer in eastern China. The larger PR and FAR for WBGT is related to its smaller natural variability (e.g., Fig. 1a vs Fig. 1b) and thus stronger warming-to-noise ratio. As a result, a small shift in the mean of the distribution can cause large change in the probability of extremely hot WBGT summers. Other factors such as the definition of study region and fingerprinting analysis details may also play some role.

One possible concern may be that the spread of reconstructed probability distributions is wider than the spread in the summer mean WBGT anomalies observed during the 2006–15 or 2011–20 decades (curves vs red tick marks in Fig. 5). One should not, however, expect the limited observations within a short time period, such as 10 or 30 years, to fully sample the inherent internal variability in summer mean WBGT. To do so more

adequately, we add each of the 1961–2015 residuals of observed summer mean WBGT after removing a linear trend to each of the 5-yr mean anomalies observed during a studied period (e.g., 1961–90), resulting in a set of reconstructed observations for that period, but based purely on observations (blue, gray, and black tick marks in Fig. 5 for the three studied periods), that account for low-frequency internal variability in the 50-yr observational record. It turns out that our reconstructed probability distributions indeed capture the observed variability reasonably well during the three studied periods. The slightly wider spread of the reconstructed distributions is likely due to the uncertainty in the scaling factors, as can be seen from the results based on the scaling-factor best estimate in Fig. S3 in the online supplemental material.

d. China's summer WBGT in the coming decades

How will summer mean WBGT change in the coming decades in China? We explore the change based on observation-constrained projections of future summer mean WBGT under the RCP4.5 and 8.5 emissions scenarios, where the constraint is based on the scaling factor from the one-signal fingerprinting analysis. For each region, we consider 1) the likelihood of experiencing summer mean WBGT greater than the historical (1961–2015) record value in each future decade up to the 2070s and 2) the median summer mean WBGT in these decades, which can also be interpreted as the summer mean WBGT value that will occur once every 2 years in the corresponding decade.

As expected, dramatic increases in summer WBGT are projected to continue into the coming decades (Fig. 6). By 2040s, it is projected that it will be over 4000 and 400 times as likely to experience a summer with WBGT that is as high as or higher than the historical record value relative to the 1961–90 baseline period under RCP8.5 for western and eastern China, respectively (Figs. 6a,d). It follows that almost every summer will be at least as hot as the hottest WBGT summer on record (Figs. 6b,e). Note that the probability ratio of the historical record WBGT saturates after the 2040s at a level equal to the return period of the historical record during the baseline period (dashed vertical lines in Figs. 6a and 6d) and that the return period of the historical record correspondingly approaches a lower bound of 1 year (dashed vertical lines in Figs. 6b and 6d). This means that the entire summer mean WBGT distribution is projected to shift completely above the historical record by the 2040s.

Once saturated, the probability ratio and return period of the historical record WBGT provide no information about further changes to summer WBGT and thus conditions conducive to potential heat stress risk.

We therefore study the evolution of the median summer WBGT in the future decades, expressed as anomalies relative to the 1961–90 baseline climatology (Figs. 6c,f). Under RCP8.5, the median WBGT is projected to be about 1.5°C above the baseline climatology in the 2020s in western China and in the 2030s in eastern China (the first vertical lines in Figs. 6c and 6d). For both regions, a 2.0°C warming (relative to 1961–90) in median summer mean WBGT is projected to be reached no later than the 2040s (the second vertical lines in Figs. 6c and 6d), and a 3.0°C warming is projected to occur around 2060s (the third vertical lines in Figs. 6c and 6d), again with warming in western China being substantially faster than in eastern China. The increases in the median summer WBGT under RCP4.5 are comparable to or slightly smaller than the corresponding increases under RCP8.5 by the 2030s (see Fig. S4 in the online supplemental material for the RCP4.5 results). Warming under RCP4.5 is considerably slower beyond the 2030s, indicating the benefits of emissions reductions in reducing summer WBGT in China. It should, however, be noted that even the aggressive emissions reductions that would be required to achieve RCP4.5 are unlikely to prevent a warming of 2.0°C in the median of summer mean WBGT relative to 1961–90 by the 2060s.

Should these projected changes in summer WBGT actually occur, they could have substantial impacts on the public health in China. Warming in seasonal mean WBGT will translate to a shift of the daily WBGT distribution to warmer levels, leading to the occurrence of more heat days that are more conducive to potential heat stress risk. It is recognized that human heat stress depends not only on thermal environmental conditions but also on human exposure, which is largely related to adaptation measures such as the use of air conditioning. Nevertheless, although adaptation could reduce human exposure to heat stress conditions, it will not affect the occurrence of those conditions, leading to substantial increases in cooling energy demand as well as damaging impacts on outdoor laborers, people in rural areas with limited heat adaptation resources, and livestock.

We note that by applying the ALL scaling factor to future projections, that is, using the so-called Allen, Stott, and Kettleborough (ASK) method (Stott and Forest 2007), we implicitly assume that the fractional errors in the model simulations of the summer mean WBGT changes in western and eastern China stay constant over time. This means that the method is best suited for constraining projections of future climate during the period of strong transient response to external forcings, but that it is less well suited for stabilization or overshoot scenarios such as RCP2.6. We therefore chose to focus on projections under RCP8.5 and RCP4.5 scenarios that are more consistent with the ASK assumption than RCP2.6, particularly
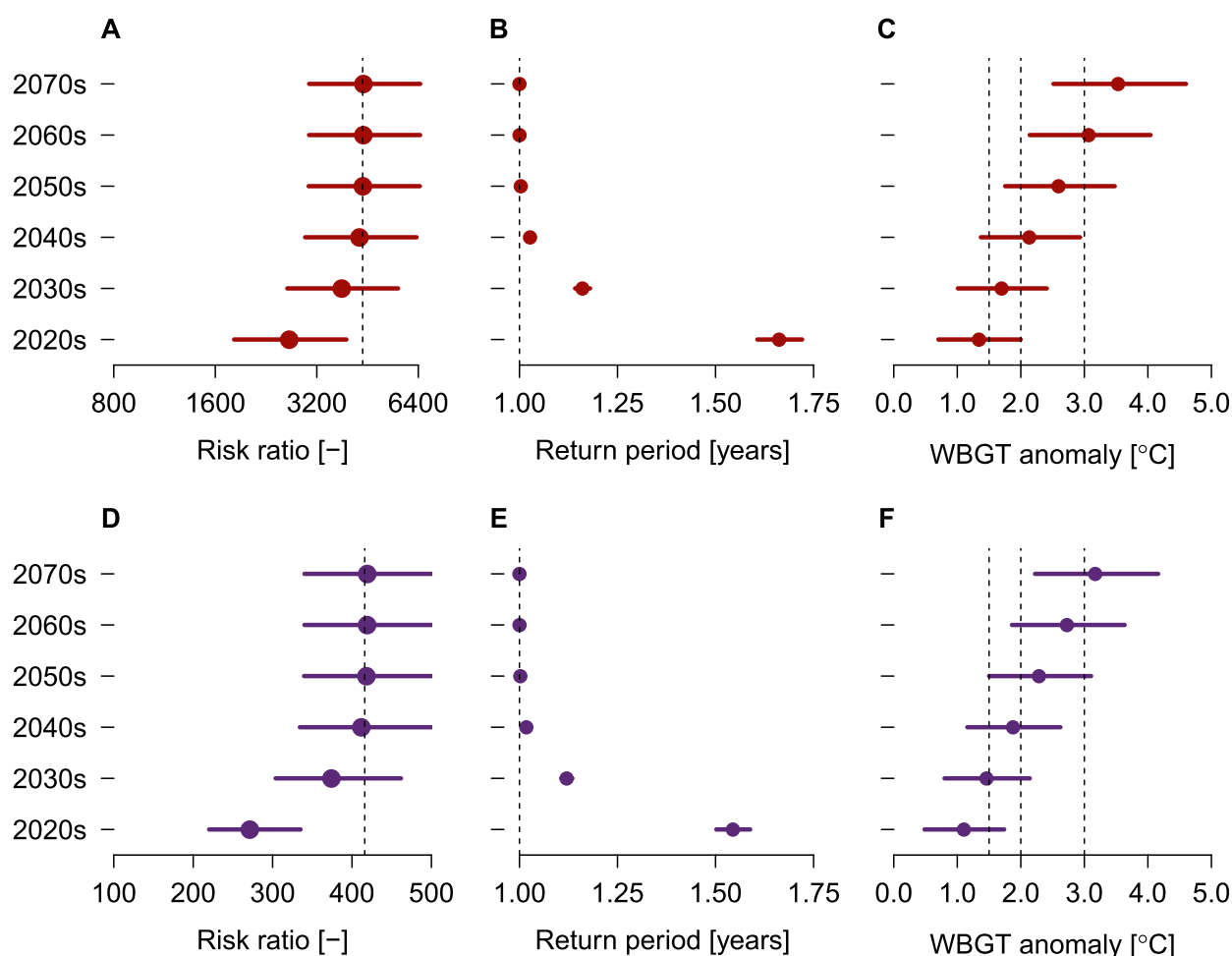
FIG. 6. Human influence is projected to continue to shift the probability distribution of summer mean WBGT to hotter levels, leading to more frequent hot summers that are more conducive to more extreme heat stress: (left) the estimated risk ratios for the record summer mean WBGT experienced during 1961–2015 in future decades relative to the 1961–90 baseline period, (center) the return periods of the record summer mean WBGT, and (right) the distributions of summer mean WBGT for (a)–(c) western and (d)–(f) eastern China, as based on observation-constrained projections under RCP8.5 forcing scenarios. Points in (a), (b), (d), and (e) show the best estimates, and the whiskers extend to the 5%–95% uncertainty ranges of the corresponding measures. Points in (c) and (f) show the medians of the observation-constrained summer mean WBGT distributions, and the whiskers mark the 5%–95% ranges of the distributions. Vertical lines in (a), (b), (d), and (e) mark the levels at which the corresponding measures are saturated, and those in (c) and (f) indicate different warming levels (i.e., 1.5°, 2.0°, and 3.0°C) relative to the 1961–90 baseline period.

for the period up to the 2060s. Nevertheless, changes to summer mean WBGT in both regions are found to scale reasonably well with changes in global mean annual mean surface air temperature (see also Willet and Sherwood 2012). This means that given the observation-constrained projections under RCP8.5 (or RCP4.5) scenario and based on the warming levels under RCP2.6, one can roughly infer the corresponding results for RCP2.6.

5. Conclusions

Benefiting from the newly available quality-controled and homogenized dataset for near-surface air temperature

and relative humidity over China, we have presented a first comprehensive evaluation of changes in summer mean WBGT in China for a period extending from 1961 to late this century. In addition to air temperature, WBGT integrates relative humidity as well and thus more closely reflects potential changes in heat stress risk. Moreover, WBGT has lower variance and a higher warming-to-noise ratio than dry air temperature. Therefore, humans and livestock perceive changes in WBGT more quickly than the same changes in air temperature. The relatively smaller variance in WBGT can also render the increased level of thermal discomfort associated with any increase in WBGT to be more persistent than that associated

with the same increase in air temperature. These facts emphasize the importance of evaluating current and projected changes in summer WBGT in China.

Summer mean WBGT is found to have increased by 1.17°C during 1961–2010 in western China and by 0.70°C in eastern China. On the basis of rigorous space–time fingerprinting analyses, we confirm that these increases can be explained by human influence on the climate, while natural influence is negligible. We find that these human-induced long-term increases in summer mean WBGT have exerted substantial influence on the occurrence of extreme hot summers. We estimate that the hottest summers on record during 1961–2015 have been made about 1100 and 140 times as likely in the present decade 2011–20 relative to the 1961–90 baseline period in western and eastern China, respectively, by human influence on the climate. From observation-constrained projections of future summer mean WBGT under RCP8.5, we find that by the 2040s almost every summer is projected to be at least as hot as the hottest summer on record during 1961–2015 in both regions and by the 2060s more than 50% of summers are projected to be about 3.0°C hotter than the 1961–90 climatology in these regions.

We note that our fingerprinting analysis results may be subject to some uncertainties as a result of the possible effects of the compensation biases in the observations that are affected by the rapid urbanization in China, and those in the model-simulated response signals to the assumed external forcings that favor more warming during last decade. In addition, because of the lack of high-quality observations and simulations of wind speed, solar radiation, and surface pressure, our estimates of WBGT represent well-shaded or non-airconditioned indoor conditions. At the time of writing, homogenized daily time series of relative humidity observations are not yet available. We therefore have to analyze summer mean WBGT estimated from monthly mean air temperature and relative humidity. These estimates therefore do not well reflect conditions conducive to peak heat stress risk during summers. Whether the heat stress–conducive conditions reflected by summer mean WBGT would result in heat stress on humans or livestock depends largely on social adaption, which we do not address in this study. We emphasize, however, that adaptation could reduce exposure to potential heat stress risk but it cannot affect the occurrence of such conditions, leading to substantial increases in cooling energy demand as well as damaging impacts on outdoor laborers, livestock, and people in rural areas with limited heat adaptation resources.

REFERENCES

Akihiko, T., Y. Morioka, and S. K. Behera, 2014: Role of climate variability in the heatstroke death rates of Kanto region in Japan. *Sci. Rep.*, **4**, 5655, https://doi.org/10.1038/srep05655.

Allen, M. R., and P. A. Stott, 2003: Estimating signal amplitudes in optimal fingerprinting: I. Theory. *Climate Dyn.*, **21**, 477–491, https://doi.org/10.1007/s00382-003-0313-9.

——, ——, J. F. B. Mitchell, R. Schnur, and T. L. Delworth, 2000: Quantifying the uncertainty in forecasts of anthropogenic climate change. *Nature*, **407**, 617–620, https://doi.org/10.1038/35036559.

Argüeso, D., A. Di Luca, S. E. Perkins-Kirkpatrick, and J. P. Evans, 2016: Seasonal mean temperature changes control future heat waves. *Geophys. Res. Lett.*, **43**, 7653–7660, https://doi.org/10.1002/2016GL069408.

Budd, G. M., 2008: Wet-bulb globe temperature (WBGT)—Its history and its limitations. *J. Sci. Med. Sport*, **11**, 20–32, https://doi.org/10.1016/j.jsams.2007.07.003.

Buzan, J. R., K. Oleson, and M. Huber, 2015: Implementation and comparison of a suite of heat stress metrics within the Community Land Model version 4.5. *Geosci. Model Dev.*, **8**, 151–170, https://doi.org/10.5194/gmd-8-151-2015.

Cai, M., and J. Lu, 2007: Dynamical greenhouse-plus feedback and polar warming amplification. Part II: Meridional and vertical asymmetries of the global warming. *Climate Dyn.*, **29**, 375–391, https://doi.org/10.1007/s00382-007-0238-9.

Cao, L., Y. Zhu, G. Tang, and Z. Yan, 2016: Climatic warming in China according to a homogenized data set from 219 stations. *Int. J. Climatol.*, **36**, 4384–4392, https://doi.org/10.1002/joc.4639.

Christidis, N., P. A. Stott, F. W. Zwiers, H. Shiogama, and T. Nozawa, 2012: The contribution of anthropogenic forcings to regional changes in temperature during the last decade. *Climate Dyn.*, **39**, 1259–1274, https://doi.org/10.1007/s00382-011-1184-0.

CMA, 2018: China Climate Bulletin 2018. China Meteorological Administration, http://www.cma.gov.cn/root7/auto13139/201903/t20190319_517664.html.

Coffel, E. D., R. M. Horton, and A. de Sherbinin, 2018: Temperature and humidity based projections of a rapid rise in global heat stress exposure during the 21st century. *Environ. Res. Lett.*, **13**, 014001, https://doi.org/10.1088/1748-9326/aaa00e.

Davies-Jones, R., 2008: An efficient and accurate method for computing the wet-bulb temperature along pseudoadiabats. *Mon. Wea. Rev.*, **136**, 2764–2785, https://doi.org/10.1175/2007MWR2224.1.

Dunne, J. P., R. J. Stouffer, and J. G. John, 2013: Reductions in labour capacity from heat stress under climate warming. *Nat. Climate Change*, **3**, 563–566, https://doi.org/10.1038/nclimate1827.

Fischer, E. M., and R. Knutti, 2012: Robust projections of combined humidity and temperature extremes. *Nat. Climate Change*, **3**, 126–130, https://doi.org/10.1038/nclimate1682.

——, K. W. Oleson, and D. M. Lawrence, 2012: Contrasting urban and rural heat stress responses to climate change. *Geophys. Res. Lett.*, **39**, L03705, https://doi.org/10.1029/2011GL050576.

Fyfe, J. C., N. P. Gillett, and F. W. Zwiers, 2013a: Overestimated global warming over the past 20 years. *Nat. Climate Change*, **3**, 767–769, https://doi.org/10.1038/nclimate1972.

——, K. von Salzen, J. N. S. Cole, N. P. Gillett, and J.-P. Vernier, 2013b: Surface response to stratospheric aerosol changes in a coupled atmosphere–ocean model. *Geophys. Res. Lett.*, **40**, 584–588, https://doi.org/10.1002/grl.50156.

Gao, J., Y. Sun, Q. Liu, M. Zhou, Y. Lu, and L. Li, 2015: Impact of extreme high temperature on mortality and regional level definition of heat wave: A multi-city study in China. *Sci. Total Environ.*, **505**, 535–544, https://doi.org/10.1016/j.scitotenv.2014.10.028.

Ghatak, D., E. Sinsky, and J. Miller, 2014: Role of snow-albedo feedback in higher elevation warming over the Himalayas, Tibet Plateau and Central Asia. *Environ. Res. Lett.*, **9**, 114008, https://doi.org/10.1088/1748-9326/9/11/114008.

Gillett, N. P., V. K. Arora, G. M. Flato, J. F. Scinocca, and K. von Salzen, 2012: Improved constraints on 21st-century warming derived using 160 years of temperature observations. *Geophys. Res. Lett.*, **39**, L01704, https://doi.org/10.1029/2011GL050226.

Goldie, J., S. C. Sherwood, D. Green, and L. Alexander, 2015: Temperature and humidity effects on hospital morbidity in Darwin, Australia. *Ann. Global Health*, **81**, 333–341, https://doi.org/10.1016/j.aogh.2015.07.003.

Gu, S., C. Huang, L. Bai, C. Chu, and Q. Liu, 2016: Heat-related illness in China, summer of 2013. *Int. J. Biometeor.*, **60**, 131–137, https://doi.org/10.1007/s00484-015-1011-0.

Harrington, L. J., and F. E. L. Otto, 2018: Adapting attribution science to the climate extremes of tomorrow. *Environ. Res. Lett.*, **13**, 123006, https://doi.org/10.1088/1748-9326/aaf4cc.

Heo, S., and M. L. Bell, 2018: Heat waves in South Korea: Differences of heat wave characteristics by thermal indices. *J. Exposure Sci. Environ. Epidemiol.*, **29**, 790–805, https://doi.org/10.1038/s41370-018-0076-3.

——, ——, and J.-T. Lee, 2019: Comparison of health risks by heat wave definition: Applicability of wet-bulb globe temperature for heat wave criteria. *Environ. Res.*, **168**, 158–170, https://doi.org/10.1016/j.envres.2018.09.032.

Hyatt, O. M., B. Lemke, and T. Kjellstrom, 2010: Regional maps of occupational heat exposure: Past, present, and potential future. *Global Health Action*, **3**, 5715, https://doi.org/10.3402/gha.v3i0.5715.

Huntingford, C., P. A. Stott, M. R. Allen, and F. H. Lambert, 2006: Incorporating model uncertainty into attribution of observed temperature change. *Geophys. Res. Lett.*, **33**, L05710, https://doi.org/10.1029/2005GL024831.

IPCC, 2013: *Climate Change 2013: The Physical Science Basis*. Cambridge University Press, 1535 pp., https://doi.org/10.1017/CBO9781107415324.

Jones, G. S., P. A. Stott, and N. Christidis, 2013: Attribution of observed historical near-surface temperature variations to anthropogenic and natural causes using CMIP5 simulations. *J. Geophys. Res. Atmos.*, **118**, 4001–4024, https://doi.org/10.1002/jgrd.50239.

Kang, S., and E. A. B. Eltahir, 2018: North China Plain threatened by deadly heatwaves due to climate change and irrigation. *Nat. Commun.*, **9**, 2894, https://doi.org/10.1038/s41467-018-05252-y.

Knutson, T. R., and J. J. Ploshay, 2016: Detection of anthropogenic influence on a summertime heat stress index. *Climatic Change*, **138**, 25–39, https://doi.org/10.1007/s10584-016-1708-z.

Lemke, B., and T. Kjellstrom, 2012: Calculating workplace WBGT from meteorological data. *Ind. Health*, **50**, 267–278, https://doi.org/10.2486/indhealth.MS1352.

Li, C., X. Zhang, F. W. Zwiers, Y. Fang, and A. M. Michalak, 2017: Recent very hot summers in Northern Hemispheric land areas measured by wet bulb globe temperature will be the norm within 20 years. *Earth's Future*, **5**, 1203–1216, https://doi.org/10.1002/2017EF000639.

——, Y. Fang, K. Caldeira, X. Zhang, N. S. Diffenbaugh, and A. M. Michalak, 2018: Widespread persistent changes to temperature extremes occurred earlier than predicted. *Sci. Rep.*, **8**, 1007, https://doi.org/10.1038/s41598-018-19288-z.

Liao, W., and Coauthors, 2018: Stronger contributions of urbanization to heat wave trends in wet climates. *Geophys. Res. Lett.*, **45**, 11 310–11 317, https://doi.org/10.1029/2018GL079679.

Liljegren, J. C., R. A. Carhart, P. Lawday, S. Tschopp, and R. Sharp, 2008: Modeling the wet bulb globe temperature using standard meteorological measurements. *J. Occup. Environ. Hyg.*, **5**, 645–655, https://doi.org/10.1080/15459620802310770.

Ma, C., Y. Honda, and T.-N. Dang, 2018: Comparison of wet-bulb globe temperature (WBGT) and mean temperature for assessment of heat-related mortality. *Japan. J. Health Human Ecol.*, **84**, 52–72, https://doi.org/10.3861/kenko.84.2_52.

Medhaug, I., M. B. Stolpe, E. M. Fischer, and R. Knutti, 2017: Reconciling controversies about the 'global warming hiatus'. *Nature*, **545**, 41–47, https://doi.org/10.1038/nature22315.

Pal, J. S., and E. A. B. Eltahir, 2015: Future temperature in southwest Asia projected to exceed a threshold for human adaptability. *Nat. Climate Change*, **6**, 197–200, https://doi.org/10.1038/nclimate2833.

Pepin, A. C., and Coauthors, 2015: Elevation-dependent warming in mountain regions of the world. *Nat. Climate Change*, **5**, 424–430, https://doi.org/10.1038/nclimate2563.

Ren, G., and Y. Zhou, 2014: Urbanization effects on trends of extreme temperature indices of national stations over mainland China, 1961–2008. *J. Climate*, **27**, 2340–2360, https://doi.org/10.1175/JCLI-D-13-00393.1.

——, Y. Ding, Z. Zhao, J. Zheng, T. Wu, G. Tang, and Y. Xu, 2012: Recent progress in studies of climate change in China. *Adv. Atmos. Sci.*, **29**, 958–977, https://doi.org/10.1007/s00376-012-1200-2.

Ribes, A., S. Planto, and L. Terray, 2013: Application of regularized optimal fingerprinting to attribution. Part I: Method, properties and idealised analysis. *Climate Dyn.*, **41**, 2817–2836, https://doi.org/10.1007/s00382-013-1735-7.

Ridley, D. A., and Coauthors, 2014: Total volcanic stratospheric aerosol optical depths and implications for global climate change. *Geophys. Res. Lett.*, **41**, 7763–7769, https://doi.org/10.1002/2014GL061541.

Sen, P. K., 1968: Estimates of the regression coefficient based on Kendall's tau. *J. Amer. Stat. Assoc.*, **63**, 1379–1389, https://doi.org/10.1080/01621459.1968.10480934.

Sherwood, S. C., and M. Huber, 2010: An adaptability limit to climate change due to heat stress. *Proc. Natl. Acad. Sci. USA*, **107**, 9552–9555, https://doi.org/10.1073/pnas.0913352107.

Shiogama, H., D. Stone, S. Emori, K. Takahashi, S. Mori, A. Maeda, Y. Ishizaki, and M. R. Allen, 2016: Predicting future certainty constraints on global warming projections. *Sci. Rep.*, **6**, 18903, https://doi.org/10.1038/srep18903.

Stott, P. A., and J. A. Kettleborough, 2002: Origins and estimates of uncertainty in predictions of twenty-first century temperature rise. *Nature*, **416**, 723–726, https://doi.org/10.1038/416723a.

——, and C. E. Forest, 2007: Ensemble climate predictions using climate models and observational constraints. *Philos. Trans.*

Roy. Soc., **A365**, 2029–2052, https://doi.org/10.1098/rsta.2007.2075.

Stull, R., 2011: Wet-bulb temperature from relative humidity and air temperature. *J. Appl. Meteor. Climatol.*, **50**, 2267–2269, https://doi.org/10.1175/JAMC-D-11-0143.1.

Sun, Y., X. Zhang, F. W. Zwiers, L. Song, H. Wan, T. Hu, H. Yin, and G. Ren, 2014: Rapid increase in the risk of extreme summer heat in eastern China. *Nat. Climate Change*, **4**, 1082–1085, https://doi.org/10.1038/nclimate2410.

——, ——, G. Ren, F. W. Zwiers, and T. Hu, 2016: Contribution of urbanization to warming in China. *Nat. Climate Change*, **6**, 706–709, https://doi.org/10.1038/nclimate2956.

——, T. Hu, X. Zhang, C. Li, C. Lu, G. Ren, and Z. Jiang, 2019: Contribution of global warming and urbanization to changes in temperature extremes in Eastern China. *Geophys. Res. Lett.*, **46**, 11 426–11 434, https://doi.org/10.1029/2019GL084281.

Taylor, K. E., R. J. Stouffer, and G. A. Meehl, 2012: An overview of CMIP5 and the experiment design. *Bull. Amer. Meteor. Soc.*, **93**, 485–498, https://doi.org/10.1175/BAMS-D-11-00094.1.

Wan, H., X. Zhang, F. W. Zwiers, and S. Min, 2015: Attributing northern high-latitude precipitation change over the period 1966–2005 to human influence. *Climate Dyn.*, **45**, 1713–1726, https://doi.org/10.1007/s00382-014-2423-y.

Wang, Y., Y. Sun, T. Hu, D. Qin, and L. Song, 2017: Attribution of temperature changes in western China. *Int. J. Climatol.*, **38**, 742–750, https://doi.org/10.1002/joc.5206.

Wehner, M., F. Castillo, and D. Stone, 2017: The impacts of moisture and temperature on human health in heat waves. Oxford Research Encyclopedias, Natural Hazard Science, https://doi.org/10.1093/acrefore/9780199389407.013.58.

Willett, K. M., and S. Sherwood, 2012: Exceedance of heat index thresholds for 15 regions under a warming climate using the wet-bulb globe temperature. *Int. J. Climatol.*, **32**, 161–177, https://doi.org/10.1002/joc.2257.

——, R. J. H. Dunn, P. W. Thorne, S. Bell, M. Podesta, D. E. Parker, P. D. Jones, and C. N. Williams, 2014: HadISDH land surface multi-variable humidity and temperature record for climate monitoring. *Climate Past*, **10**, 1983–2006, https://doi.org/10.5194/cp-10-1983-2014.

Zhao, Y., A. Durcharne, B. Sultan, P. Braconnot, and R. Vautard, 2015: Estimating heat stress from climate-based indicators: Present-day biases and future spreads in the CMIP5 global climate model ensemble. *Environ. Res. Lett.*, **10**, 084013, https://doi.org/10.1088/1748-9326/10/8/084013.

Zhu, J., S. Wang, and G. Huang, 2019: Assessing climate change impacts on human-perceived temperature extremes and underlying uncertainties. *J. Geophys. Res. Atmos.*, **124**, 3800–3821, https://doi.org/10.1029/2018JD029444.